Front. Electr. Electron. Eng. China (2006) 2: 234–238
DOI 10.1007/s 11460-006-0015-2

RESEARCH ARTICLE

YANG Jun, YUAN Li-bo

Theoretical and experimental study on white light interferometric sensing network with double-ring topology

Abstract A white-light interferometric fiber-optic sensing network based on the double-ring topology is demonstrated, which can be applied to the measurements of quasi-distributed strain and temperature in a smart structure. In order to increase the multiplexing capacity, decrease the measurement cost of each sensor, and improve the ability of reliability of the sensor network, a double-port interrogating technology was used. The double- ring fiber optical sensing network based on the space division multiplexing (SDM) is further developed. The low coherent multiplexing principle in the double-ring network structure is analyzed. Based on the optical path matching condition of SDM, the intensity characteristic of the interference signal in the sensor is deduced. The characteristics of the double-ring sensing network connecting 9 sensors and its property of robust resisting destruction are verified by experiments, and the results are analyzed and discussed**.**

Keywords Fiber optics, Multiplexing, Double-ring topology structure, Sensing network

1 Introduction

The low-coherence interferometric [1] fiber-optic sensor system has a large multiplexing capacity [2], which has been widely use analyzed in the past 20 years. Many kinds of multiplexing technologies have been developed [3] including the multiplexing technology of sensing systems in series [3-4], in parallel [5] or with a loop topology [6-7]. The ratio of output signals to noise and the multiplexing capacity for the white-light interferometric fiber-optic sensing systems can be greatly enhanced through the improvement of the system configuration [3,8], which has been demonstrated both theoretically and experimentally. In this paper, a white-light interferometric sensing network with double-ring topology is presented. By resorting to the double-port interrogating technology, the measurement cost of each individual sensor is reduced and the ability of reliability resist destruction of the sensor network is improved. This enables the sensing system to be more suitable for the measurement of distributed strain or temperature.

Translated from *Acta Optical Sinica*, 2005, 25(6) (in Chinese)

YANG Jun, YUAN Li-Bo(✉)
Department of Physics, Harbin Engineering University, Harbin 150001, China

2 Principle of white-light interferometry

A typical configuration of a white-light interferometer is shown in Fig. 1.

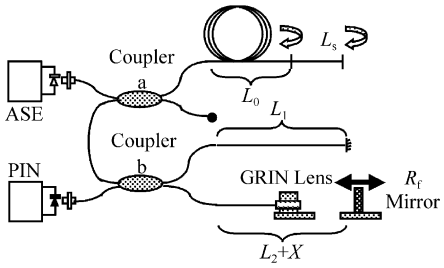

Fig. 1 Configuration of white-light interferometer

where a and b are two 2×2 3 dB SMF couplers (insertion loss is α_a and α_b, respectively), L_s is the length of the fiber sensor gauge. A Michelson-based optical path demodulator (MOPD) is connected to coupler a. Inside the MOPD, the light is split into two arms by coupler b. The length of the reference arm is L_1 and the reflectivity of its mirrored fiber end is R_f; L_2 is the length of the optical scanning arm, and it is constituted of a GRIN lens and a scanning mirror with its reflectivity R_g and insertion loss $\eta(x)$.

In the sensing system the broad width spectral light from an amplified spontaneous emission (ASE) light source is

launched into the sensing arm L_0 through coupler a. Reflected light beams from the two fiber sensor ends 1 and 2 are guided into the MOPD between which there is the optical path difference (OPD). The light signals are coupled into the reference arm and the optical scanning arm and then reflected by the mirrored end and the scanning mirror, respectively, and finally led to a photodiode. The OPD of the Michelson interferometer can be adjusted with a scanning mirror to match and trace the change in the fiber length in each sensing segment. We make the OPD of the Michelson interferometer nearly equal to the fiber sensor gauge length so that the two reflected light waves from the two ends of each sensing gauge can be matched with each other. When the OPD of the Michelson interferometer is equal to the gauge length of a particular sensor, a white-light fringe pattern is produced. The central fringe, which is located in the center of the fringe pattern and has the highest amplitude peak, is an exact match of the OPD for that sensor. The OPD-matching condition is given [9] by:

$$n_0\Delta L + X = n_0 L_s \tag{1}$$

where $\Delta L=L_2 - L_1$ is the length difference of the two arms in the Michelson interferometer, X is the distance between the reflective mirror and the GRIN Lens, and n_0 is the fiber mode refractive index. Therefore, we can measure the deformation of a sensor by tracing the change in mirror displacement ΔX:

$$\Delta X = \Delta(n_0 L_s) \tag{2}$$

If the optical path of the fiber sensor is modulated by an ambient perturbation, for instance, strain or temperature, then the perturbation parameters related to the optical path change will be measured and recorded by the shift in the interference signal peak.

The intensity of output signals of the white-light interferometer can be given [9] by:

$$I = I_1 + I_2 + 2\sqrt{I_1 I_2}\,|\gamma(x)|\cos(kx+\phi) \tag{3}$$

where I_1, I_2 are the intensity of two light beams, k is the wave number, x is the OPD of the two beams, ϕ is the original phase, $\gamma(x)$ is the light self-coherent function.

Distinguishing from the central band is used in gaining the white-light interferometric signals. We take the maximum intensity of output signals, $I_{\text{am-max}}$, as a special sign that the OPD for the sensor is exactly matched. According to Eq. (1), $I_{\text{am-max}}$ is given [5–8] by:

$$I_{\text{am}-\max} = 2I_0\left(\frac{\alpha_a}{2}\right)^2\left(\frac{\alpha_b}{2}\right)^2 RT\beta\sqrt{R_g R_f \eta(x)} \tag{4}$$

where I_0 is the intensity of the light source, R, T and β are the reflectivity, the transmission and the insertion loss of the sensor surfaces 1 and 2, respectively. R_f, R_g are the reflectivity of the optical scanning mirror and the mirrored end in the reference arm, respectively, $\eta(x)$ is the function of the insertion loss versus the location of the scanning mirror.

3 Configuration of double-ring network

White-light interferometer is good at multiplexing. For the multiplexed fiber-optic sensors, if the gauge lengths of the fiber sensors satisfy the following conditions: $l_i \neq l_j$ and $l_i - l_j \geq L_c$, there is only a single white-light interferometric signal for each different sensor, where L_c is the coherence length of the amplified spontaneous emission light source. Within the optical scanning range, the multiplexing technology based on the isolation of the interferemetric signals can be called space division multiplexing (SDM).

Based on SDM, a double-ring fiber optical sensor network in series is demonstrated, as shown in Fig.2. Where 3 dB coupler c is connected to coupler a and results in two ring resonators d and e in geometry.

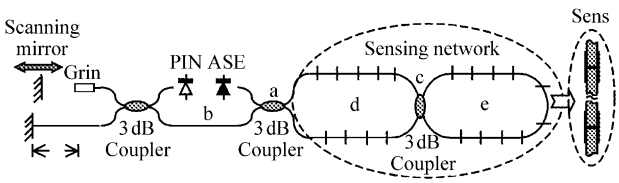

Fig. 2 Low-coherent fiber optic interferometer based on double-ring network topological structure

There are m, n sensors arrayed in the upper and lower arms of the ring d, respectively, and p of that in the ring e. The sensor gauge length is l_1, l_2,⋯, l_m, l_1, l_2,⋯, l_n and l_1, l_2,⋯, l_p, respectively. The arrangement of sensors in the double-ring network and the demonstration of signal analysis are shown in Fig.3. The lines marked with the number in the rings are the reflective surfaces of the sensors, for the kth of which, the reflectivity is R_k, and T_k is the transmission and β_k is the insertion loss.

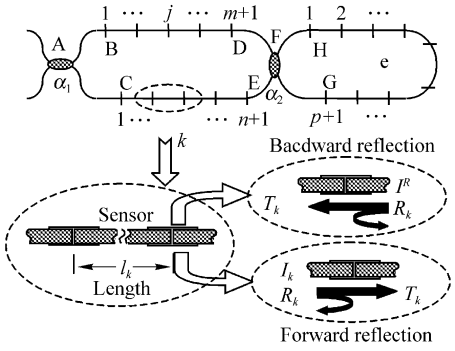

Fig. 3 Arrangement of sensors in the double-ring network and the demonstration of signal analysis

4 Characters of signals

The analysis of the signals for bi-directional transmission properties is complicated in the complex double-ring network. Chances are that the upper arm and lower arm in

ring d are symmetric and the bi-directional transmissions in ring e are equal, thus the problem is greatly simplified.

The maximum amplitude of the output signals, $I_{\text{am-max}}$, introduced above, can be drawn using path tracing method. With the assumption that:

1) The length of the sensor k is l_k, the average length of the sensors is l_0, and the difference is small, i.e., $l_k \approx l_0$; for any two different sensors k, j, the length are not equal, i.e., $l_k \neq l_j$.

2) The couplers a, b and c are all 3 dB couplers, and the insertion loss are α_1, α_2 and α_3, respectively.

3) For the reflective sensor end k, the reflectivity, the transmission and the insertion loss are equal for the bi-directional light signals.

Thus, for the sensor k in the upper arm of ring d, $I_{\text{am-max}}$ can be given by:

$$I_{j,j+1} = I_0 \alpha_{s,j} (\frac{\alpha_1}{2})^2 \left\{ \left[\prod_{i=2}^{j} (T_i \beta_i)^2 \right] \sqrt{R_j R_{j+1} (T_j \beta_j)^2} + \frac{(\alpha_3 \alpha_{\text{ACF}} / 2)^2}{(1 - \alpha_3 \alpha_e / 2)^2} \left[\prod_{i=j+2}^{m+1} (T_i \beta_i)^2 \right] \sqrt{R_j R_{j+1} (T_{j+1} \beta_{j+1})^2} \right\}$$

$$\prod_{i}^{j} (T_i \beta_i)^2 = 1, \quad i > j, \quad j = 1, 2, \cdots, m+1 \tag{5}$$

For the sensor j in the lower arm of ring d, $I_{\text{am-max}}$ can also be given by:

$$I_{k,k+1} = I_0 \alpha_{s,k} (\frac{\alpha_1}{2})^2 \left\{ \left[\prod_{i=2}^{k} (T_i \beta_i)^2 \right] \sqrt{R_k R_{k+1} (T_k \beta_k)^2} + \frac{(\alpha_3 \alpha_{\text{ACF}} / 2)^2}{(1 - \alpha_3 \alpha_e^2 / 2)^2} \left[\prod_{i=k+2}^{n+1} (T_i \beta_i)^2 \right] \sqrt{R_k R_{k+1} (T_{k+1} \beta_{k+1})^2} \right\}$$

$$\prod_{i}^{j} (T_i \beta_i)^2 = 1, \quad i > j, \quad k = 1, 2, \cdots, n+1 \tag{6}$$

For the sensor j in the ring e, $I_{\text{am-max}}$ can be given by:

$$I_{j,j+1} = I_0 \frac{\alpha_{s,j} (\alpha_1 \alpha_3 / 4)^2}{(1 - \alpha_a \alpha_e / 2)^2} \left\{ \alpha_{\text{ACF}}^2 \sqrt{R_j R_{j+1} (T_j \beta_j)^2} \left[\prod_{i=2}^{j} (T_i \beta_i)^2 \right] + \alpha_{\text{ACF}}^2 \sqrt{R_j R_{j+1} (T_{j+1} \beta_{j+1})^2} \left[\prod_{i=j+2}^{m+1} (T_i \beta_i)^2 \right] \right\}$$

$$\prod_{i}^{j} (T_i \beta_i)^2 = 1, \quad i > j, \quad j = 1, 2, \cdots, p+1 \tag{7}$$

where I_0 is the intensity of the light from the light source; α_{ABF}, α_{ACF} and α_{e} are loss factors as the light signals passing through the upper arm of ring d, the lower arm of ring d and ring e, respectively, which can be defined as: $\alpha_{\text{ABF}} = \prod_{i=1}^{m+1} (T_i \beta_i)$, $\alpha_{\text{ACF}} = \prod_{i=1}^{n+1} (T_i \beta_i)$ and $\alpha_e = \prod_{i=1}^{p+1} (T_i \beta_i)$; $\alpha_{s,j}$ is the loss factor introduced by the MPOD for the sensor k, and it is defined as $\alpha_{s,j} = (\alpha_2 / 2)^2 (R_{\text{f}} R_{\text{g}} \eta(x, x_{j+1}))^{1/2}$, $\eta(x, x_{j+1})$ is the insertion loss caused by the scanning mirror at the location related to the sensor k.

To simplify the problem, the reflectivity R, transmission T and insertion loss β of the sensors are 0.02, 0.88 and 0.9, respectively, equal to all sensors. The simulation results of the output signal characteristic in a double-ring sensing network is plotted in Fig. 4. The intensity of the light from the ASE light source, I_0, is 0 dbm (1 mW).

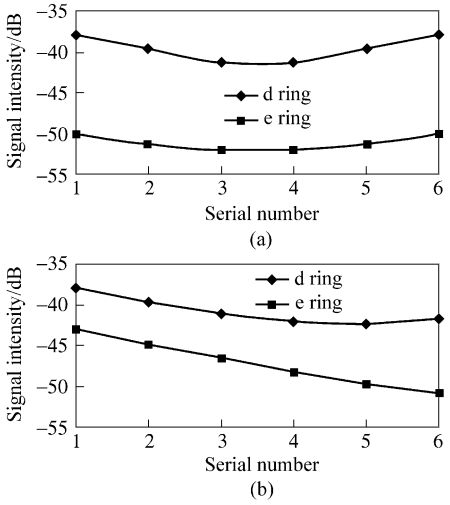

Fig. 4 Simulation results of the output signal characteristic in a double-ring sensing network

There are 12 sensors in the double-ring network, with six in ring d and the other six in ring e. In Fig. 4(a), 3 sensors are arrayed in the upper arm and the other 3 in the lower arm, while in Fig. 4(b) 6 sensors are all arrayed in the upper arm or the lower one. We can see in Fig. 4 that the output signals of the sensors in ring d are more significant than that in ring e; and the output signals of sensors in ring **e** are influenced by the distribution of the sensors in ring d because of the total loss of signals in ring d.

5 Experimental results and analysis

In the experimental setup shown in Fig. 2, the light source power is 0 dBm at a wavelength of 1 550 nm with a 40 nm bandwidth. The scanning range is 400 mm in air, and the average insertion loss is approximately 5 dB with a fluctuation of less than 0.2 dB. A total of nine fiber sensors are linked in the two-loop network by butt connectors, and the arrangement of fiber optic sensors is depicted in Fig. 5; the gauge length of each sensor is approximately 510 mm, as shown in Table 1. The serial sensors S1– S9, are located in the upper and lower arms in ring d and ring e, each with 3. *L*1–*L*5 are just fibers connecting the sensors and the couplers. A series of simulations with damage to various sensors were performed to investigate the robustness of the double-ring sensing network. The output characteristic of double-ring sensing network is shown in Fig. 6, which is in good agreement with the theoretical calculation. The difference in intensity results from the difference in reflectivity of the sensor end.

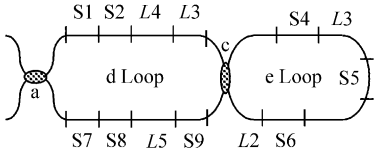

Fig. 5 Demonstration of fiber optic sensor connecting location

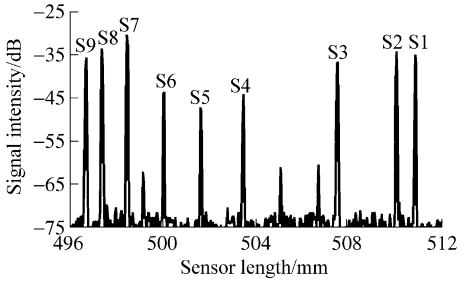

Fig. 6 Output characteristic of double-ring sensing network

Table 1 Fiber optic sensors length /mm

number	Length/mm	number	Length/mm
*S*1	510.89	S6	500.05
*S*2	510.10	S7	498.47
*S*3	507.53	S8	497.42
*S*4	503.56	S9	496.74
*S*5	501.66		

Figs. 7–9 show the variation of the intensity output results corresponding to the breaking points *L*1, *L*2 and *L*3. It can be seen that the nine sensors are still functional no matter whether there is damage or not, except that the amplitude of some of the signals is lower than before.

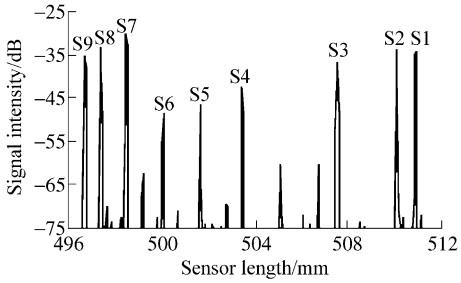

Fig. 7 Output characteristic of sensing network with opened *L*1

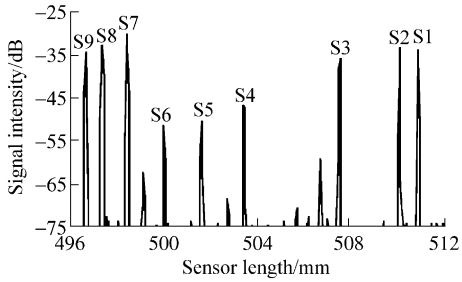

Fig. 8. Output characteristic of double-ring network with opened *L*2

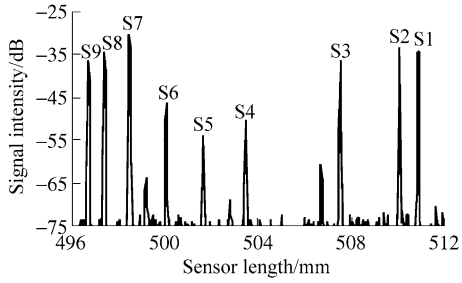

Fig. 9 Output characteristic of double-ring with opened *L*3

For the case of two breaking points the test results are depicted in Figs. 11-12: If the breaking points are *L*1 and *L*2, although the double-ring network has been destroyed, the nine-sensor system is still working, as shown in Fig. 10, while the signal intensity of sensors S4, S5 and S6 is greatly reduced. If the breaking points are *L*3 and *L*4, it can be seen from Fig. 11 that the output signals of sensors S5 and S6 vanish and the amplitude of the signal from sensor S4 is reduced. If the breaking points are *L*3 and *L*5, not only is the amplitude of the signals from sensors S5 and S6 reduced but also that of the sensor S6, and sensor S4 is invalid, as shown in Fig. 12.

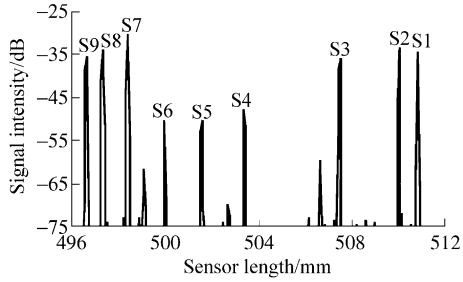

Fig. 10 Output characteristic of sensing network with opened *L*1 and *L*2

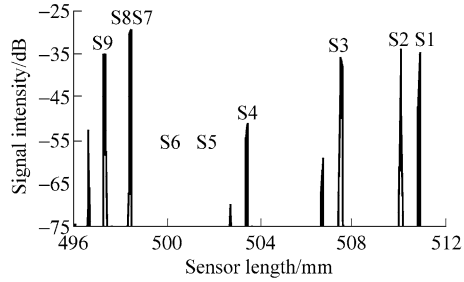

Fig. 11 Output characteristic of sensing network with opened *L*3 and *L*4

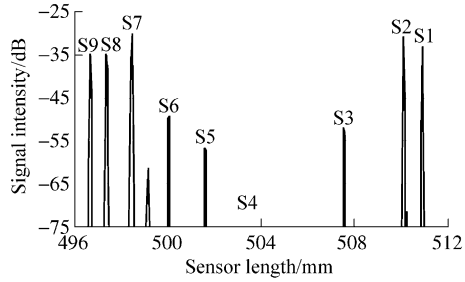

Fig. 12 Output characteristic of sensing network with opened *L*3 and *L*5

6 Conclusions

In summary, a multiplexed fiber-optic deformation sensor double-ring network that is suitable for smart-structure applications has been designed and demonstrated. Such a double-ring topology is useful in constructing a sensor network for distributed strain or temperature measurement in smart structures. This double-ring network architecture greatly improves the reliability of the system and provides redundancy owing to the double-ring topology. This means

that, even if a part of the sensor double-ring network breaks down, the system will still work. Compared with fiber-optic sensor single-ring topology, the reliability of the double-ring system has been further improved; that is when the double-ring sensor network system has been broken at two points on the fiber sensor chain simultaneously, most of the sensors are still working well. This avoids failure of the whole sensing system owing to local damage of the sensor integrated structure.

Acknowledgements This work was supported by the Teaching and Research Award Program for Outstanding Young Professors in Higher Education Institute from the Ministry of Education of China and National Natural Science Foundation of China (No. 60577005).

References

1. Born M., Wolf E, Principles of optics, 6th ed (New York: Pergamon) 1980
2. Brooks J, Wentworth R, Youngquist R.Tur, Coherence multiplexing of fiber-optic interferometric sensors, Lightwave Technology, 1985, 3(5):1062 –1072
3. Sorin, W.V., Baney, D.M., Multiplexed sensing using optical low-coherence reflectometry, IEEE Photonics Technology Letters, 1995 ,7(8):917 –919
4. Stefan McMurtry, John D. Wright, David A. Jackson, A multiplexed low coherence interferometric system for humidity sensing, Sensors and Actuators B , 2000, 67 (1-2):52–56
5. Libo Yuan, Limin Zhou, 1×N star coupler as distributed fiber optic strain sensor in a white light interferometer, Applied Optics, 1998, 37(19)：4168–4172
6. Libo Yuan, Wei Jin, Limin Zhou, et al., Enhanced multiplexing capacity of low-coherence reflectometric sensors with a loop topology, IEEE photonics technology letters, 2002, 14(8)：1157–1159
7. Libo Yuan, Limin Zhou , Wei Jin, et al.. Design of a fiber-optic quasi-distributed strain sensors ring network based on a white-light interferometric multiplexing technique, Appled Optics , 2002, 41(34)：7205–7211
8. Jiang Jian, Rao Yuanjiang, Ren Zengling, et al., A novel extrinsic fiber-optic fabry-perot interferometric sensing system based on optical amplification, Acta Optica Sinica，2004，24（2）：183–186（in chinese）
9. Rao,Y.J., Jackson, D.A., Recent progress in fibre optic low-coherence interferometry, Meas. Sci. Technol, 1996, 7(7): 981–999